Solid-State Electronics 199 (2023) 108506

Contents lists available at ScienceDirect

Solid State Electronics

journal homepage: www.elsevier.com/locate/sse

An atomistic modeling framework for valence change memory cells ☆

Manasa Kaniselvan, Mathieu Luisier, Marko Mladenović *

Integrated Systems Laboratory, ETH Zurich, CH-8092 Zurich, Switzerland

ARTICLE INFO

Keywords:
Valence change memory
RRAM
Memristors
Dielectric breakdown
Kinetic Monte Carlo
Quantum transport

ABSTRACT

We present a framework dedicated to modeling the resistive switching operation of Valence Change Memory (VCM) cells. The method combines an atomistic description of the device structure, a Kinetic Monte Carlo (KMC) model for the creation and diffusion of oxygen vacancies in the central oxide under an external field, and an *ab initio* quantum transport method to calculate electrical current and conductance. As such, it reproduces a realistically stochastic device operation and its impact on the resulting conductance. We demonstrate this framework by simulating a switching cycle for a TiN/HfO_2/TiN VCM cell, and see a clear current hysteresis between high/low resistance states, with a conductance ratio of one order of magnitude. Additionally, we observe that the changes in conductance originate from the creation and recombination of vacancies near the active electrode, effectively modulating a tunneling gap for the current. This framework can be used to further investigate the mechanisms behind resistive switching at an atomistic scale and optimize VCM material stacks and geometries.

1. Introduction

Neuromorphic computing units require the development of solid-state synapses that are often realized in the form of devices with adjustable electrical conductance. Amongst such devices are valence change memory (VCM) cells. These are two-terminal metal-oxide-metal stacks across which applied voltages can drive the creation of oxygen vacancies and their redistribution into a conductive filament — an applied voltage of the opposite polarity can then partially dissolve the filament, thus breaking the conductive pathway across the oxide. The resulting conductance can then be measured with a low readout voltage without further disrupting the defect arrangement. VCMs are both relatively straightforward to fabricate and exhibit an especially large dynamic range.

The mechanisms behind resistive switching in VCM have been studied in detail [1], but simulation of these devices is complicated by the stochasticity of their operation and the atomistic granularity of the resulting conductance. The movement of oxygen vacancies has been modeled using Kinetic Monte Carlo (KMC) methods [2,3] or Molecular Dynamics (MD) simulations [4], and the microscopic nature of bonding across the defective interfaces of a VCM filament has been investigated at the *ab initio* level [5]. Previous simulation frameworks which attempt to describe the full device-level operation of VCM typically combine these methods with trap-assisted tunneling models of current flow [2,6,7]. However, the required equations are derived for single trap energies, and may not fully describe transport through the inhomogeneous defect distribution in a VCM. Capturing both atomic rearrangement and realistic transport properties necessitates a more fundamental level of theory.

Here we present a framework dedicated to modeling VCM. Our method relies on a stochastic Kinetic Monte Carlo (KMC) model parameterized with density functional theory (DFT), followed by *ab initio* quantum transport simulations, all of which are preformed on the same atomic grid. It thus captures the growth and dissolution of oxygen vacancy filaments through the VCM cell and the electrical current that flows through them.

2. Modeling framework

Fig. 1 shows a schematic of the nominal VCM cell considered: an amorphous HfO_2 oxide with TiN electrodes. The amorphous oxide is initially generated by melting and cooling it from the monoclinic phase using MD. In this process a block of monoclinic HfO_2 is first melted at 3000 K for 300 ps, then cooled to 300 K at a rate of 9 K/ps, and finally annealed for 50 ps, all performed under an NVT thermostat with the LAMMPS code [8]. The atomic interactions during this process are characterized by a ReaxFF force-field for Hf-O systems [9]. The purpose behind this MD step is to generate a realistically randomized starting structure; to remove any remaining coordination defects and

☆ The review of this paper was arranged by Francisco Gamiz.

* Corresponding author.
E-mail address: mmladenovic@iis.ee.ethz.ch (M. Mladenović).

https://doi.org/10.1016/j.sse.2022.108506

Available online 4 November 2022

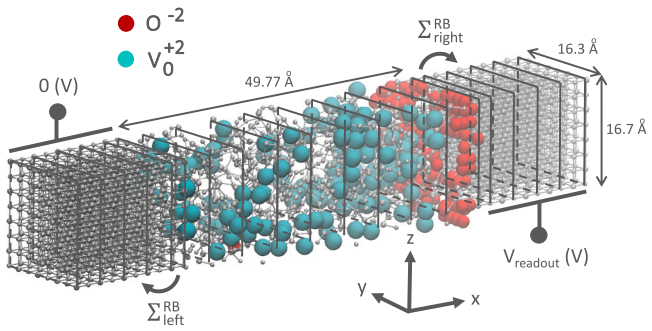

Fig. 1. Atomic structure of a typical metal-oxide-metal VCM cell. Oxygen vacancies (V_0^{+2}) and oxygen ions (O^{-2}) are pictured with larger blue and red spheres, respectively. The device is partitioned into 'blocks' of atoms representing the underlying block-structure of the Hamiltonian (H_{cp2k}) and overlap (S_{cp2k}) matrices in Eq. (2). (For interpretation of the references to color in this figure legend, the reader is referred to the web version of this article.)

unrealistic bond lengths, the cell size and atomic positions of the annealed structure are relaxed using the cp2k DFT code [10]. TiN electrodes are then attached along the transport direction. The interface distance between TiN and HfO_2 is optimized in cp2k to provide the lowest energy.

Next, oxygen vacancy (V_O^{+2}) and ion (O^{-2}) rearrangements under an applied voltage (V_{app}) are modeled with an in-house KMC code. KMC has been used previously to model physical processes governed by the harmonic transition state theory [11], and is capable of reproducing realistically stochastic behavior [12]. The inputs to this model are a selected set of events which can occur in the oxide, as well as the corresponding activation energies which would need to be overcome to execute them. Here we consider four types of events: (1) vacancy/ion pair generation, (2) vacancy/ion pair recombination, (3) vacancy diffusion (in which a vacancy exchanges lattice positions with an oxygen atom), and (4) oxygen ion diffusion (in which an oxygen ion moves between interstitial sites in the lattice). An event is then selected from this set once per timestep. The selection probability $P_{i,j}^x$ of event 'x' occurring between locations (or 'sites') 'i' and 'j' in the oxide is given by

$$P_{i,j}^x = \nu \cdot exp\left(-\frac{E_A^x - E_{i,j}}{k_B T}\right), \tag{1}$$

where E_A^x is the zero-field activation energy of event x, and ν is an attempt frequency [3]. The sites involved in each event are restricted to being within a predefined neighbor radius of one another. The zero-field activation energies E_A^x are found for amorphous HfO_2 through DFT calculations, using the Nudged Elastic Band (NEB) method. We assume a reduced activation energy for vacancy generation at the interface with the active (top) electrode, which in our model plays the role of an exchange layer/reservoir into which ions can be transferred and stored. This reduced energy for interface generation has been reported previously [13,14], and can be attributed to the increased likelihood of separating oxygen ions from under-coordinated hafnium. The energy is reduced only at the top interface to model the presence of an oxidizable electrode, which is typically added to one end of the switching layer to collect migrating oxygen vacancies. Subtracted from the activation energy is the energy provided by the applied field $E_{i,j} = q \cdot (\phi_i - \phi_j)$, considering the charge (q) and potential (ϕ) for each pair of sites involved. Clustered vacancies are presumed conductive and first set to a charge state of zero (V_O^0). ϕ at each site is then determined by treating the oxide as a network of nodes across which V_{app} dissipates.

The KMC algorithm makes a list whose elements k_x correspond to the cumulative sum of event probabilities $P_{i,j}^n$, $n = 1 \cdots x$ and chooses the first element of the list that is greater than the sum of all event probabilities k_N, multiplied by a random number r, $r \in (0, 1)$. The corresponding event $P_{i,j}^x$ is thus chosen to occur. The event selection-and-execution process repeats until the simulation timescale reaches the intended duration for which V_{app} is applied. A device snapshot is finally generated, containing information on the atomic species and positions. Fig. 2 presents an overview of this model.

To calculate the conductance of each snapshot, we use the Quantum Transmitting Boundary Method (QTBM) as implemented in the OMEN code [15,16]. Coherent transport occurs through states $\psi(E)$, which are found by solving:

$$(E \cdot S_{cp2k} - H_{cp2k} - \Sigma^{RB}(E)) \cdot \psi(E) = Inj(E) \tag{2}$$

Here, $Inj(E)$ describes carrier injection from the contacts, which are coupled to the device through $\Sigma^{RB}(E)$. H_{cp2k} and S_{cp2k} are the Hamiltonian and overlap matrices, respectively, as produced with cp2k for each of the KMC snapshots. Due to the localized nature of the underlying Gaussian-type orbitals, H_{cp2k} and S_{cp2k} have a block-structure representing atomic layers as pictured in Fig. 1. The O^{-2} ions are not included in electronic structure calculations.

3. Results

We apply this model to simulate the operation of a TiN/HfO_2/TiN VCM cell. The HfO_2 oxide has a cross-section of 1.67 x 1.63 nm^2, for a total of 2252 atoms. Starting from a structure with a formed filament (Fig. 3a), a V_{app} of −2 V is applied to switch to the high resistance state (HRS, Fig. 3b). V_{app} = 5 V is then applied to the HRS to recover a low resistance state (LRS, Fig. 3c). Vacancies and ions are shown in blue and red spheres, respectively, and artificially enlarged for visual clarity. In each case, the duration of V_{app} is 10 ms.

During the transition from the initial structure in Fig. 3a to the HRS in Fig. 3b, recombination of oxygen ions with vacancies near the active electrode results in a local dissolution of the filament, creating a tunneling gap. A transition back to the LRS in Fig. 3c occurs when a sufficiently high V_{app} regenerates vacancy/ion pairs in this gap. Fig. 4a shows the potential for the HRS and LRS structures, as used during the KMC process. The steeper electric potential across the tunneling gap in the HRS increases the likelihood of vacancy regeneration in this area, assisting in the HRS-to-LRS transition. The difference in the transmission function between these two states is pictured in Fig. 4b, and is highest near the conduction band of HfO_2, consistent with the location of V_O^{+2} vacancy defect states at this energy range [17].

Fig. 5 plots a full switching cycle, showing both the current (Fig. 5a) and conductance (Fig. 5b) at each intermediate V_{app}. The device has a current hysteresis typical of VCM, with a conductance ratio of ∼10. In the HRS and LRS, the conductance values are relatively constant, indicating their non-volatility. The asymmetry in the V_{app} between the HRS and the LRS transitions stems from the length of the conductive filament being lower in the initial device than in the final LRS, (see Fig. 3a/c), and from the recombination of V_O^{+2}/O^{-2} being far more energetically favorable than their generation.

The modeled switching dynamics are entirely dependent on the input energies and atomic grid, without any constraints on filament growth. This makes it uniquely suited for exploring the effects of atomic structure and material properties on switching performance, and for comparing different material stacks. However, there are several limitations to the approach presented here. First, although the mechanisms of bipolar resistive switching are primarily field-driven [18], local fluctuations in temperature may play a role in expediting events near the end of the filament, where the electric field is highest [19]. Our model does not consider these effects since the current is not solved self-consistently with the atomic site-resolved temperature — the computational cost associated with doing so would be exorbitant with our transport simulations. Nevertheless, we believe that the inclusion of a temperature loop would not change the fundamental physics

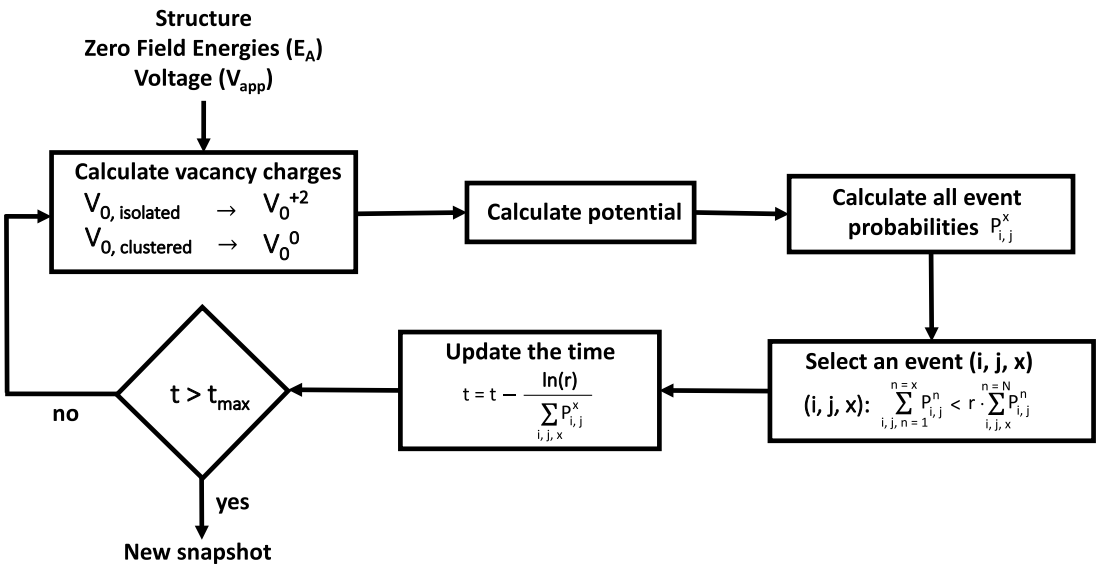

Fig. 2. Flowchart of the developed Kinetic Monte Carlo model which determines the state of atomic rearrangement under V_{app}, where r represents a random number. The final snapshot of the device is generated at time t_{max}. $P^x_{i,j}$ is calculated according to Eq. (1).

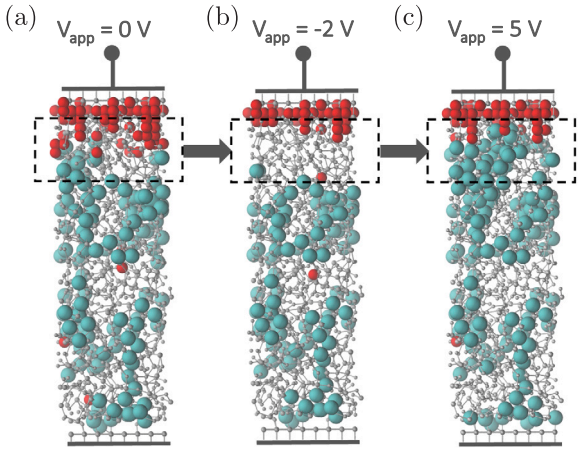

Fig. 3. Properties of the high (HRS) and low (LRS) resistance states of the TiN/HfO_2/TiN VCM cell during a single switching cycle. V_O^{+2} and O^{-2} positions along the oxide are shown for **(a)** the formed filament, **(b)** the HRS, and **(c)** the LRS. The areas near the active electrode, where the filament length varies most with the V_{app}, are indicated with dashed boxes.

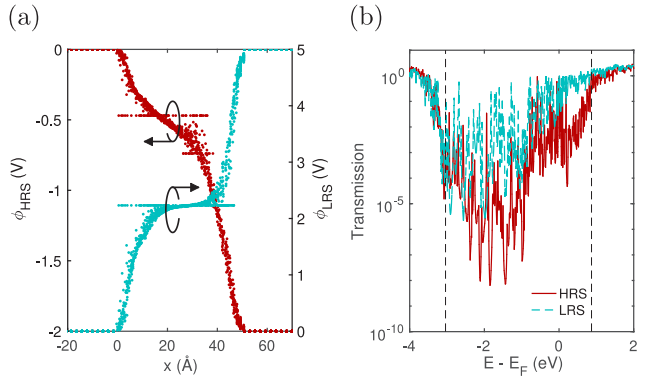

Fig. 4. Electrostatic potential (ϕ) along the oxide for the HRS (red) and LRS (blue) from Fig. 3(b-c). The HfO_2 oxide spans from 0 Åto 50 Å. **(c)** Transmission through the HRS and LRS states. The dashed lines indicate the estimated bandgap of the HfO_2 layer. (For interpretation of the references to color in this figure legend, the reader is referred to the web version of this article.)

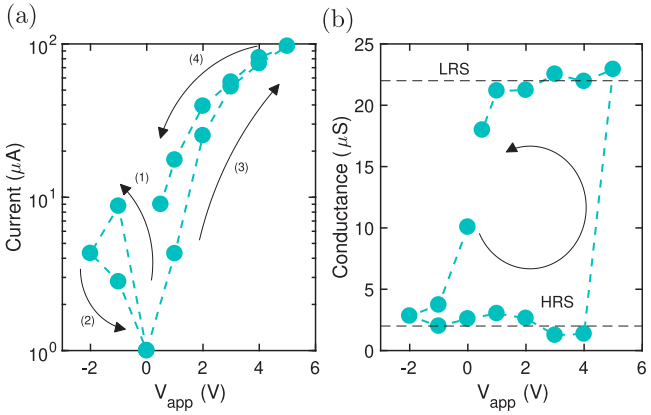

Fig. 5. Current **(a)** and conductance **(b)** of the device shown in Fig. 3 during a switching cycle, from the initial filament (0 V) to the HRS (−2 V) and finally to the LRS (5 V).

behind this field-driven switching process, and would primarily affect the magnitude of the SET/RESET voltages and the timescales at which the resistive switching occurs [1]. Finally, the structure used here is also significantly smaller than that of most experimental VCM cells, which limits the size and diameter of the filament it can host. While it can simulate memristive behavior in ultimately-scaled limits and benchmark materials, the model is not suitable to explore the possibility of multiple filaments, or the effects of various parameters on filament width.

4. Conclusion

We combined KMC and *ab initio* quantum transport on an atomic lattice to model resistive switching in a VCM cell. Our model is able to capture a non-volatile switching mechanism dominated by vacancy generation and recombination at the active electrode, resulting in a clear conductance hysteresis with an ON/OFF ratio of one order of magnitude. This framework can be used to provide insight towards the optimization of VCM material stacks and geometries.

Declaration of competing interest

The authors declare that they have no known competing financial interests or personal relationships that could have appeared to influence the work reported in this paper.

Data availability

Data will be made available on request.

Acknowledgments

We acknowledge funding from SNSF, Switzerland Sinergia (grant no. 198612), the Werner Siemens Stiftung Center for Single-Atom Electronics and Photonics, Switzerland, the Natural Sciences and Engineering Research Council of Canada (NSERC) Postgraduate Scholarship, as well as computational resources from the Swiss National Supercomputing Center (CSCS) under project 1119.

References

[1] Dittmann R, Menzel S, Waser R. Nanoionic memristive phenomena in metal oxides: The valence change mechanism. Adv Phys 2021;70(2):155–349. http://dx.doi.org/10.1080/00018732.2022.2084006.

[2] Padovani A, Larcher L, Woo J, Hwang H. A multiscale modeling approach for the simulation of OxRRAM devices. In: 2017 17th non-volatile memory technology symposium. IEEE; 2017, http://dx.doi.org/10.1109/NVMTS.2017.8171306.

[3] Zeumault A, Alam S, Wood Z, Weiss RJ, Aziz A, Rose GS. TCAD modeling of resistive-switching of HfO_2 memristors: Efficient device-circuit co-design for neuromorphic systems. Front Nanotechnol 2021;3:734121. http://dx.doi.org/10.3389/fnano.2021.734121.

[4] Urquiza ML, Islam MM, van Duin ACT, Cartoixà X, Strachan A. Atomistic insights on the full operation cycle of a HfO_2-based resistive random access memory cell from molecular dynamics. ACS Nano 2021;15(8):12945–54. http://dx.doi.org/10.1021/acsnano.1c01466.

[5] Padilha ACM, McKenna KP. Structure and properties of a model conductive filament/host oxide interface in HfO_2-based ReRAM. Phys Rev Mater 2018;2:045001. http://dx.doi.org/10.1103/PhysRevMaterials.2.045001.

[6] Bersuker G, Gilmer DC, Veksler D, Kirsch P, Vandelli L, Padovani A, et al. Metal oxide resistive memory switching mechanism based on conductive filament properties. J Appl Phys 2011;110(12):124518. http://dx.doi.org/10.1063/1.3671565.

[7] Kopperberg N, Wiefels S, Liberda S, Waser R, Menzel S. A consistent model for short-term instability and long-term retention in filamentary oxide-based memristive devices. ACS Appl Mater Interfaces 2021;13(48):58066–75. http://dx.doi.org/10.1021/acsami.1c14667.

[8] Thompson AP, Aktulga HM, Berger R, Bolintineanu DS, Brown WM, Crozier PS, et al. LAMMPS - A flexible simulation tool for particle-based materials modeling at the atomic, meso, and continuum scales. Comput Phys Comm 2022;271:108171. http://dx.doi.org/10.1016/j.cpc.2021.108171.

[9] Senftle TP, Hong S, Islam MM, Kylasa SB, Zheng Y, Shin YK, et al. The ReaxFF reactive force-field: Development, applications and future directions. Npj Comput Mater 2016;2(1):15011. http://dx.doi.org/10.1038/npjcompumats.2015.11.

[10] Kühne TD, Iannuzzi M, Ben MD, Rybkin VV, Seewald P, Stein F, et al. CP2K: An electronic structure and molecular dynamics software package - Quickstep: Efficient and accurate electronic structure calculations. J Chem Phys 2020;152(19):194103. http://dx.doi.org/10.1063/5.0007045.

[11] Henkelman G, Jónsson H. Long time scale kinetic Monte Carlo simulations without lattice approximation and predefined event table. J Chem Phys 2001;115(21):9657–66. http://dx.doi.org/10.1063/1.1415500.

[12] Andersen M, Panosetti C, Reuter K. A practical guide to surface kinetic Monte Carlo simulations. Front Chem 2019;7:202. http://dx.doi.org/10.3389/fchem.2019.00202.

[13] O'Hara A, Bersuker G, Demkov AA. Assessing hafnium on Hafnia as an oxygen getter. J Appl Phys 2014;115(18):183703. http://dx.doi.org/10.1063/1.4876262.

[14] Traore B, Blaise P, Sklenard B, Vianello E, Magyari-Kope B, Nishi Y. HfO_2/Ti interface mediated conductive filament formation in RRAM: An Ab Initio study. IEEE Trans Electron Dev 2018;65(2):507–13. http://dx.doi.org/10.1109/ted.2017.2785352.

[15] Luisier M, Schenk A, Fichtner W, Klimeck G. Atomistic simulation of nanowires in the Sp3D5S tight-binding formalism: From boundary conditions to strain calculations. Phys Rev B 2006;74(20):205323. http://dx.doi.org/10.1103/PhysRevB.74.205323.

[16] Ducry F, Aeschlimann J, Luisier M. Electro-thermal transport in disordered nanostructures: A modeling perspective. Nanoscale Adv 2020;2(7):2648–67. http://dx.doi.org/10.1039/D0NA00168F.

[17] Robertson J. High dielectric constant gate oxides for metal oxide Si transistors. Rep Progr Phys 2005;69(2):327–96. http://dx.doi.org/10.1088/0034-4885/69/2/r02.

[18] Yang JJ, Strukov DB, Stewart DR. Memristive devices for computing. Nature Nanotechnol 2012;8(1):13–24. http://dx.doi.org/10.1038/nnano.2012.240.

[19] Roldán JB, González-Cordero G, Picos R, Miranda E, Palumbo F, Jiménez-Molinos F, et al. On the thermal models for resistive random access memory circuit simulation. Nanomaterials 2021;11(5):1261. http://dx.doi.org/10.3390/nano11051261.